First principles calculations of the optical properties of C_xN_y single walled nanotubes

Debnarayan Jana[1]**, Anirban Chakraborti**[2,6]**, Li-Chyong Chen**[3]**,
Chun Wei Chen**[4] **and Kuei-Hsien Chen**[5]

[1] Department of Physics, University College of Science and Technology, University of
Calcutta, Kolkata-700 009, West Bengal, India
[2] Department of Physics, Banaras Hindu University, Varanasi-221005, India
[3] Center for Condensed Matter Sciences, National Taiwan University, Taipei 10617, Taiwan
[4] Department of Material Science and Engineering, National Taiwan University, Taipei 10617,
Taiwan
[5] Institute of Atomic and Molecular Sciences, Academia Sinica, Taipei 10617, Taiwan

E-mail: djphy@caluniv.ac.in

Abstract
The optical properties of (8, 0) single walled carbon nanotubes alloyed with nitrogen (N) have
been examined using relaxed carbon–carbon (C–C) bond length *ab initio* density functional
theory (DFT) calculations in the long wavelength limit. The maximum value of the absorption
coefficient is shown to depend strongly on the concentration of N in a non-linear way as well as
on the direction of polarization. The reflectivity at normal incidence vanishes at some unique
concentration of N. It is also observed that the peak of the loss function (in parallel polarization
and unpolarized cases) shifts to a higher frequency indicating the enhanced metallic character.
The observed variation of the plasma resonance frequencies with N concentration indicates the
existence of a unique maximum for parallel polarization and a step function like behavior for
the unpolarized situation with concentration.

(Some figures in this article are in colour only in the electronic version)

1. Introduction

Owing to their unique one-dimensional structure, carbon
nanotubes (CNTs) possess unusual physical, chemical and
mechanical properties. Quite naturally, CNTs have attracted
the attention of theoretical and experimental research
groups [1–3]. The electronic properties of single walled
carbon nanotubes (SWCNTs) depend strongly on size and
chirality. However, in the experimental synthesis of CNTs
the above properties cannot be easily tailored. But there
have been quite a few attempts to control the properties by
incorporating extrinsic foreign atom doping. In most of these
dopings, the natural choices have been boron (B) or N, for
two specific reasons. Firstly, both B and N have atomic radii

similar to C. Secondly, B- and N-doped CNTs can either be p-
type or n-type CNTs [4], similar to the usual semiconducting
materials, resulting in several important applications in
nano-electronic devices [5]. These substitutions in CNTs
significantly modify the chemical binding configuration
and physical and chemical properties in comparison to
pure CNTs.

By substituting the C atoms by B, stable new B-doped
systems have been synthesized in SWCNTs [6–8]. Moreover,
study of their electronic properties suggests that boron is in
sp^2 configuration [9]. In particular, BC_3 nanotubes have
drawn much attention from both theoretical and experimental
researchers [10]. High resolution transmission electron
microscopy (HRTEM) along with nano-electron energy loss
spectroscopy (nano-EELS) has been employed to study the
structural defects in B-doped systems [11]. A comparative
study in TEM has also been performed in B-doped systems

and BN nanotubes [12]. Besides, a theoretical calculation on B-doped systems indicates that they can act as a novel sensor for formaldehyde [13].

Recent examples have been N doping in multi-walled carbon nanotubes (MWCNTs), which introduces an appreciable atomic scale deformation [14–16] in the local network of (5, 5) and (9, 0), and the synthesis of composite $B_xC_yN_z$ tubes and reports of their electron energy loss spectroscopy (EELS) [17, 18]. Also, the electron current distribution in B- and N-doped armchair CNTs has been investigated using density functional theory (DFT) and the Green's function technique to show a chiral flow of current [19]. The doping effects on hydrogen adsorption [20] and dissociative diffusion [21] in pure and N-doped SWCNTs are important areas to identify the key sites and paths of the reaction. Moreover, it is well known that pure SWCNTs are unable to detect highly toxic gases, water molecules and bio-molecules [22]. To improve the reliability and quality of nanosensors, the importance of substitutional alloying of impurity atoms such as B and N has been discussed [23, 24]. These studies are also important from the technological point of view as doping helps to control the device design in molecular electronics and sensors. The characterization of the structure of SWCNTs on N ions reveals the appearance of n-type character on ion irradiation [25], and the stability of N-doped CNTs under electron irradiation has been explored theoretically [26]. The biological importance of toxicological effects was compared between pure MWCNTs and N-doped SWCNTs [27]. Chemical vapor deposition (CVD) growth [28] of N-doped CNTs on silicon and SiO_2 substrates and its mechanism have been proposed from x-ray photoelectron spectroscopy (XPS) and the amount of incorporated N was explored via EELS [29]. XPS combined with EELS has been used to find out the typical binding configurations [30] of N and C in N-doped SWCNTs. The enhancement of the C–N bond obtained from the photo emission spectra of chlorine treated nitrogenated SWCNTs has been explained recently through first principles calculations [31]. High purity N-doped double walled carbon nanotubes (DWCNTs) by CVD [32], N-doped CNTs by aerosol assisted CVDs [33] and radio frequency magnetron sputtering [34] and N-doped SWCNTs by floating catalyst CVDs [35] have been synthesized. The various aspects of the doping of N in CNTs have been reviewed recently [36, 37]. The template synthesis of N-doped of MWCNTs has been proposed [38]. High current density in N-doped CNTs has been observed [39] in contrast with un-doped CNTs. X-ray absorption spectroscopy has been employed to control N in N-doped MWCNTs synthesized by plasma enhanced chemical vapor deposition (PECVD) [40]. In the literature, B-doped and N-doped systems are generally designated as B_xC_y and C_xN_y, respectively, where x and y are positive prime integers. If one of the atoms in (8, 0) SWCNTs is replaced by an N atom, then the structure is known as $C_{31}N$. For 50% doping of N in SWCNTs, the model developed is termed CN. Instead of N, if 16 B atoms replace the same number of C atoms in (8, 0) SWCNTs, then BC structure is developed. Fourier transform of infrared (FTIR) studies have been performed in N-doped MWCNTS to identify

the various bonds present in the system [41]. Theoretically, the metallic character [42] of CN has been predicted by first principles calculation. Even a decrease [43] in the density of states (DOS) at the Fermi level of (5, 5) N-doped CNTs with a NH_2 group bonded to an N atom has been observed. This study is indicative of gaseous hazardous species. Also, the optical properties of 4 Å diameter pure SWCNTs have been investigated [44–46] recently by first principles calculation to explain the experimental results. Most recently, *ab initio* calculations of the linear and non-linear optical properties of pure SWCNTs have shown that [47] the dielectric function depends essentially on the chirality, diameter and the nature of polarization of the incident electromagnetic field.

All the above examples indicate that substitutional doping either by B and N in CNTs significantly influences the electronic states near the Fermi energy depending on the level of concentration of dopants. Naturally, the optical properties which depend on the band structure will be changed by the concentration. We perform here the optical calculations of single walled carbon nano-composites following DFT for low to higher levels of N concentration. Although the hypothetical systems are far away from the experimental ones and doping systems, we believe, however, that this study will shed some light on the electronic structure and collective excitations of B–C–N-alloyed SWCNTs. In particular, we would like to investigate the optical properties of (8, 0) C_xN_y nanotubes as a function of N concentration under the action of a uniform electric field with various polarization directions through relaxed C–C bond length *ab initio* DFT. This would help us to establish the differences in the optical properties of B_xC_y with the C_xN_y nanotubes. The plan of this paper is as follows: in section 2, we give a brief description of the numerical methods we have employed. In section 3, we discuss the simulation results. Finally, in section 4, we give the conclusions and perspectives of the paper.

2. Numerical methods

An extensive account of the numerical computation dealing with various aspects has been described in our earlier work [48–50] associated with a B-alloyed system. Here we briefly summarize some of the salient features of this computation. In this numerical simulation, the imaginary part of the dielectric function has been computed by using first order time dependent perturbation theory. In the simple dipole approximation used in the Cambridge serial total energy package (CASTEP) code [51], the imaginary part is given by

$$\varepsilon_2\left(q \to 0_{\vec{u}}, \hbar\omega\right) = \frac{2e^2\pi}{\Omega\varepsilon_0}$$
$$\times \sum_{k,V,C} |\langle \psi_k^C|\vec{u}\cdot\vec{r}|\psi_k^V\rangle|^2 \delta(E_k^C - E_k^V - E) \tag{1}$$

where Ω and ε_0 represent, respectively, the volume of the super-cell and the dielectric constant of the free space; $\vec{u}, \vec{r}$, respectively, represent the polarization vector of the incident electric field and position vector. The wavefunctions ψ_k^C and ψ_k^V are the corresponding conduction band (CB) and valence band (VB) eigenfunctions with eigenvalues E_k^C and
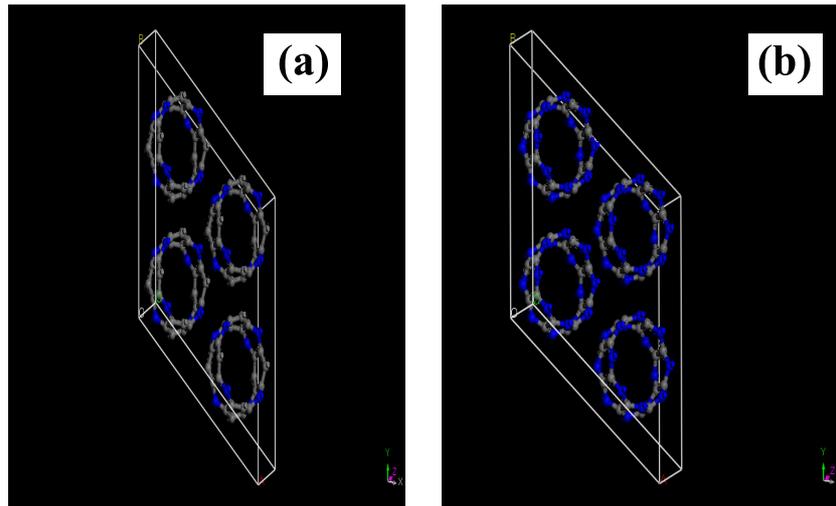
Figure 1. Ball and stick model of a (8, 0) N-doped SWCNT in a 3D triclinic structure: (a) C_3N and (b) CN.

E_k^V, respectively, obtained from the self-consistent Kohn–Sham equations [51] in the pseudo-potential formalism. At a first glance this expression looks similar to Fermi's golden rule in time dependent perturbation theory. The dielectric constant describes the typical causal response, the real and imaginary part of it are connected by a Kramers–Kronig transform. The sum over k is a crucial point in numerical calculation. The other two sums take care of the contribution of the unoccupied conduction band (CB) and occupied valence band (VB). In computing the imaginary part of the above dielectric function, typically [1/2 (total number of electrons) +4] bands were taken.

For the exchange and correlation term in DFT, the generalized gradient approximation (GGA) as proposed by Perdew *et al* [52] is adopted. The standard norm-conserving pseudo-potential in reciprocal space is invoked for the optical calculation. Compared to the standard local density approximation (LDA) (with appropriate modifications) used mostly in electronic band structure calculation, the optical properties of the system are normally standardized by *spin unpolarized* GGA. A cut-off energy of 550 eV for the grid integration was adopted for computing the charge density of the doped system. For Brillouin zone (BZ) integration along the tube axis, we have used six Monkhorst [53] k-points, a uniform grid point along the three axes in reciprocal space. The smearing broadening in computing the optical properties was kept fixed at 0.5 eV. The atomic positions are relaxed until the forces on the atoms are less than 0.01 eV $Å^{-1}$. The dielectric function for all the doped systems was computed using a $(2 \times 2 \times 5)$ Monkhorst-Pack (MP) grid for 550 eV cut-off energy. Typical convergence was achieved until the tolerance in the Fermi energy was 0.1×10^{-6} eV. Typical ball and stick models of the N-doped (8, 0) system are shown in figure 1. The geometrical structure of an impure system was built by replacing one of the C atom(s) in the hexagonal ring by N atom(s). It is important to note that the preferred N sites were chosen to have lowest total formation energy. These results are in agreement with the prediction made for N-doped $(n, 0)$ SWNT systems [54]. A schematic computational super-cell shown in figure 1 to show the various N sites (which typically includes four units of CNT) is the 3D triclinic crystal ($a = 18.801$ Å, $b = 19.004$ Å, $c = 4.219$ Å and angles $\alpha = \beta = 90°, \gamma = 120°$) having P1 symmetry. The energy cut-off, k-point sampling, geometry and GGA/norm-conserving pseudo-potential are same in all C_xN_y systems.

3. Results and discussion

3.1. Study of band structure of the C_xN_y system

Before discussing the optical properties, we schematically show the convergence of the total energy of the hypothetical structure of the CN system in figure 2. We show the logarithmic convergence of the self-consistent energy change per atom in figure 2(a) with iteration for the (8, 0) CN system, while figure 2(b) represents the convergence of the total energy of the same system. It is evident from this figure that the hypothetical structure is stable and this stability has been checked for all the systems before performing their optical calculations.

In figure 3, we schematically show the convergent band structure of the CN system. All the energies shown in this diagram have been measured with respect to the Fermi energy. For pure (8, 0) we found [48] a Fermi energy 6.028 eV with a band gap at the Γ point (the most symmetrical point in the BZ) at 0.48 eV (the energy cut-off used in the above calculation was 470 eV). The Fermi energy for CN nanotubes turns out to be 7.22 eV. We also notice that the Fermi energy (the dashed line) is within the VB and CB. It is evident from figure 3 that two bands overlap, indicating the metallic character of the (8, 0) CN tube in conformity with the (5, 5) CN tube reported earlier [55].

At lower and moderate doping concentrations, a strong overlap between the VB and CB is seen at the Z and Q points, except at the Γ point, while with high enough doping overlap continues in other k-points of the BZ. This immediately indicates the energy gap at the Γ point for the (8, 0) CN system. However, remarkably, at concentrations of N of 0.25 and 0.75, it is noticed from the band structure (not shown
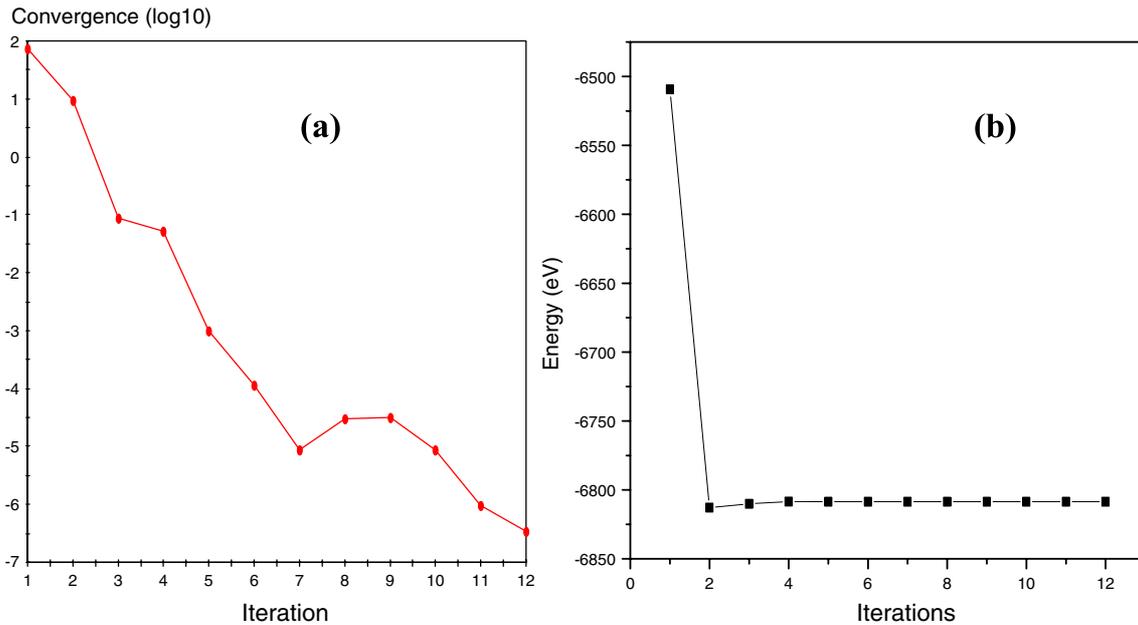
Figure 2. Convergence of the energy of the structure of the (8, 0) CN system.

in figure) that near the bottom of the VB there is a gap in energy for all values of k points in the BZ. This feature, however, does not appear at all in other N concentrations. The flatness of the band at various k-points seems to contribute significantly to the optical absorption. The partial density of states (PDOS) of the (8, 0) CN system is shown in figure 4. The figure indicates a series of spikes in the whole spectrum of band energy and these are nothing but the characteristic van Hove singularity typical feature of low-dimensional condensed matter systems. The low temperature scanning tunneling spectroscopy (STS) measurement can be used to verify the position of the spikes. It is seen that in both the pure and composite case, the contribution of p electrons in the VB is higher than its counterpart s electrons.

However, towards the bottom of the VB, the contribution of the s electrons is quite substantial in CN tubes. Compared to C atoms, the s electrons of N atoms make a significant contribution near the edge of the VB, as seen in figure 4(b).

Moreover, the contribution of p electrons at the Fermi level is greater than that of the s electrons. In fact, the higher value of the DOS at the Fermi level signifies the metallic character of CN. This behavior is in agreement with the local density of states (LDOS) calculation of N containing (5, 5) SWCNTs [55, 56]. We show in figure 5 the contribution of all the atoms (C as well as N) to the DOS. It is seen that within the energy region (-15 eV to -5 eV) in the VB, the p-type electrons make a significant contribution compared to s electrons.

Now, we concentrate on the band gap in the most symmetric point of the BZ. In figure 6, we show the schematic variation of the band gap at the Γ point of the BZ with N doping. A polynomial fit to the data obtained from the band structure calculations reveals that the maximum of the band gap is obtained at some critical concentration ($\sim$57%). This engineering of the band gap at the most symmetric point in the
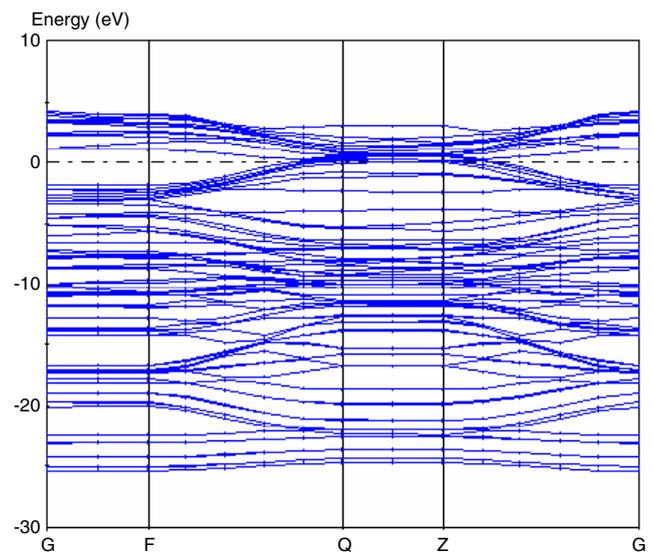

Figure 3. Band structure of the (8, 0) CN system.

BZ may be useful in device and sensor applications. However, with B doping, we noticed a minimum of the band gap [48] at the Γ point for 55% doping. These observations are required later for understanding some of the features of the optical properties of the N-alloyed CNT systems.

3.2. Study of the dielectric constant of a $C_x N_y$ system

We compute the imaginary part of the dielectric constant within the specified frequency range for a (8, 0) semiconductor as a function of N concentration at various polarization schemes including unpolarized with incidence direction (1, 0, 0). It was suggested in [44] that because of the presence of the density of scatterers in the super-cell, the imaginary dielectric constant needed to be renormalized. We believe that further
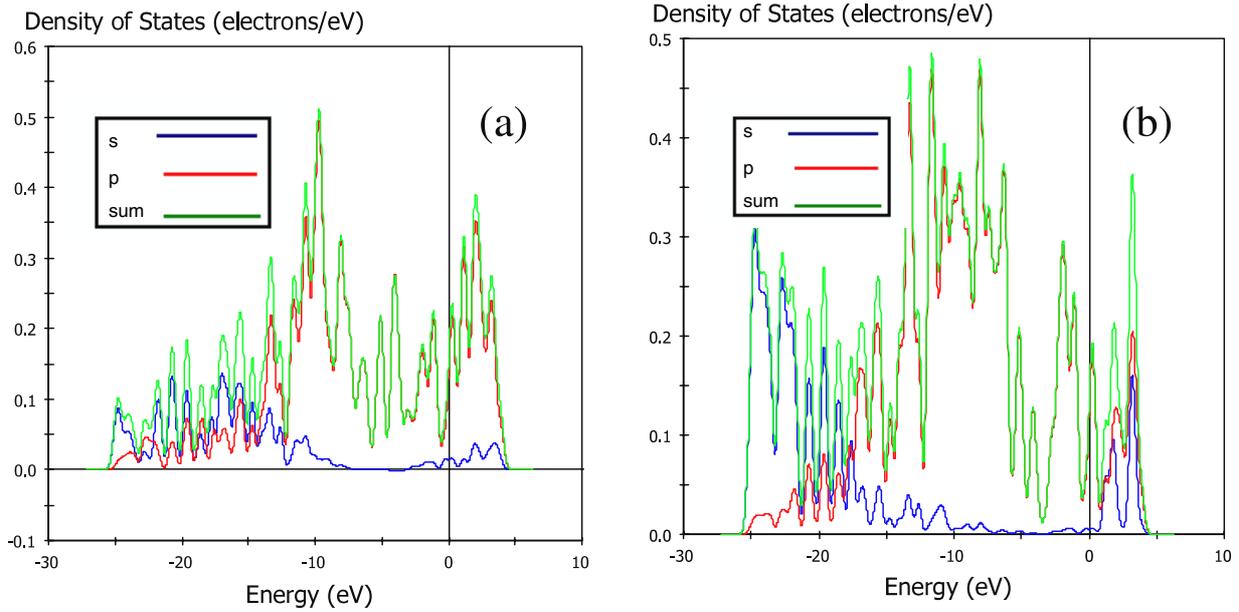
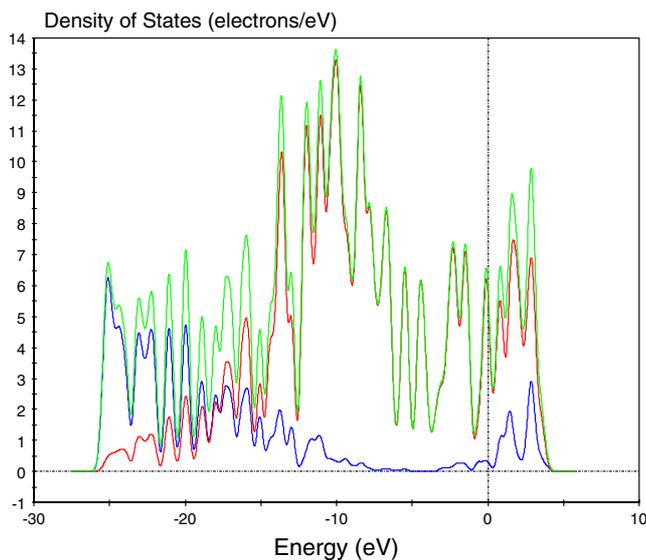**Figure 4.** Partial density of states (PDOS) of a (8, 0) CN SWCNT: (a) C atoms and (b) N atoms.

Figure 5. Partial density of states (PDOS) of a (8, 0) CN SWCNT.

Figure 6. Typical variation of the band gap at the Γ point with N concentration.

work is required to justify this renormalization procedure, and hence we do not account for such a renormalization in our calculation. In figure 7, we schematically show the dielectric constant (real as well as imaginary) for both pure (8, 0) and the CN system as a function of frequency for parallel polarization of the electromagnetic field. The parallel polarization refers to the direction of light parallel to the axis of the CNT. It is evident that in both cases the imaginary part of the dielectric constant is always positive throughout the range of frequency. This may be understood very simply from equation (1), which involves the square of the matrix element of the dot product of the polarization and position vector between the electronic states and the energy-conserving delta function. This property of ε_2 serves as one of the cross checks in our numerical computation.
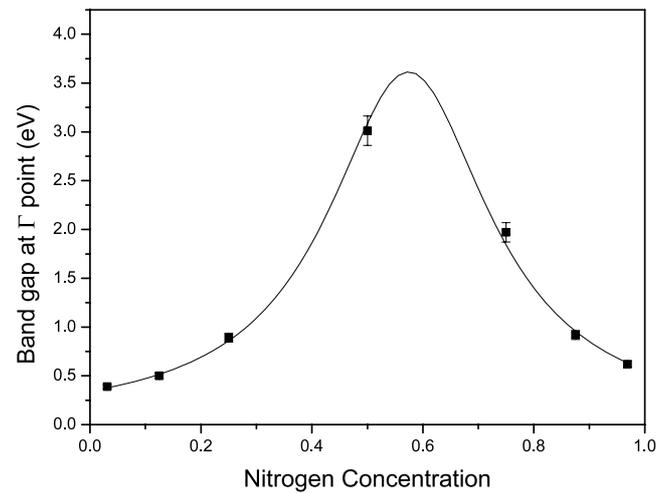
However, it is noticed from figure 7 that such a restriction is not obeyed by the real part of the dielectric constant ε_1. We also note that the static value (strictly speaking $\omega \to 0$, but in our numerical computation $\omega = 0.0100$ Hz) of the dielectric constants for both pure and doped systems is always positive. This observation is satisfied by a theorem in continuous media stating that the static electric dielectric constant is always positive [57] for any material in thermal equilibrium. The variation of the static dielectric constant with concentration of B has been reported recently [48] to show that a small concentration is enough to change the value drastically from the pure (8, 0) SWCNT. It is evident from figure 6 that the static value of the dielectric constant (real as well as imaginary) of a CN system is higher compared to the pure one. In figure 8, we show the variation of the static real dielectric constant as a
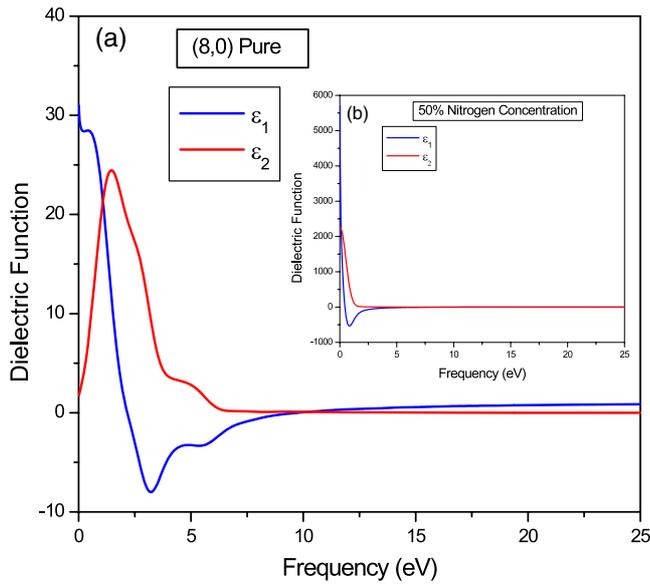
Figure 7. Typical variation of dielectric constants of (a) pure (8, 0) and (b) CN nanotube in parallel polarization as a function of frequency (ω).

Figure 8. Variation of static (real) dielectric constant with N concentration (the inset is for perpendicular polarization).

function of N concentration for all three cases. We note that the change of value of the static dielectric constant depends on both polarizations as well as on N concentration.

The respective changes in the real part of the dielectric constant with N doping concentration are significantly larger in case of parallel and unpolarized in contrast to the perpendicular case. Besides, at 50% concentration, the static real values in all three cases assume maximum values.

In the case of semiconducting SWCNTs, an *ab initio* tight-binding calculation [58, 59] relates the static value of the dielectric constant with the energy band gap as

$$\varepsilon_1(0) = 1 + \frac{(\hbar\omega_p)^2}{(5.4 E_g)^2}. \tag{2}$$

Here ω_p is the plasma frequency and E_g is the energy band gap. Based on this equation, a strong upper bound [60] to the static dielectric constant of a semiconductor SWCNT was suggested as

$$\varepsilon_1(0) < 5. \tag{3}$$

However, in our numerical calculation, the static (real) dielectric constants of all the various CNTs having a diameter of less than 1 nm violate the above inequality. This has been also noticed in another first principles calculation [44] of the optical properties of CNTs having a diameter 4 Å. Moreover, equation (2) indicates infinite static dielectric constants for pure and quasi-metallic CNTs. The infinite value is intuitively expected in view of the conducting nature [58] of the available free electrons in CNTs. However, we get *finite* positive values for pure and quasi-metallic CNTs along with their doped counterparts. We believe that the finiteness of the static values arises due to non-zero positive values of band gaps of all flavors of CNT and the small diameter of the CNT. In other words, the value of static dielectric susceptibility is increased in the doped case for this particular type of CNT.
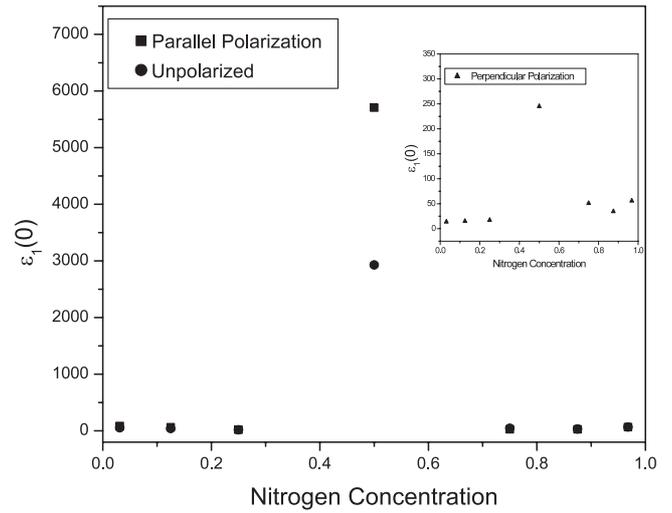
All the other optical quantities such as refractive index, optical conductivity, reflectivity, absorption coefficient and the loss function can be obtained from the dielectric constant. Below we present the variation of the absorption coefficient, reflectivity, optical conductivity and the loss function that suggests the typical nature of collective excitations of the system.

3.3. Study of the absorption spectra of N-alloyed systems

The absorption coefficient α is related to the imaginary part of the dielectric constant as

$$\alpha = \frac{\varepsilon_2 \omega}{nc} \tag{4}$$

where n and c are the refractive index and the speed of light, respectively. The absorption spectra depend crucially on the nature of the CNT and the direction of polarization. The absorption spectra are limited to the ultra-violet (UV) region only.

The existence of peaks in the spectra indicates the maximum absorption at that particular energy. With increased doping by N atom(s), both the magnitude of the peaks and their position change significantly. The appearance of several peaks in the absorption spectra in the perpendicular and unpolarized cases makes the analysis little bit complicated. In figure 9 we indicate the contrasting behavior of the absorption coefficient of a (8, 0) CN tube as function of frequency for parallel and perpendicular polarization. It is noticed that the absorption is restricted to 30 eV only and in parallel polarization, the typical absorption coefficient has a higher value compared than its perpendicular counterpart. However, more careful analysis shows that in parallel polarization, perpendicular polarization and unpolarized cases, the absorption spectra are limited to 0–25 eV. The upper limit depends crucially on the N concentration.

With the help of the most significant peaks in the absorption spectra, we compute the maximum value of the
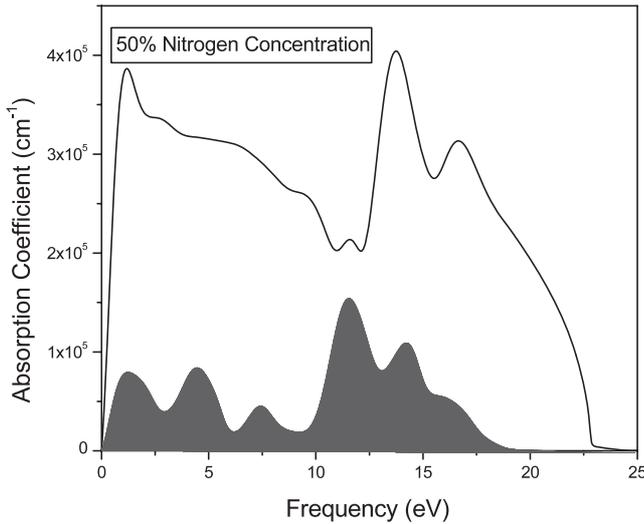
Figure 9. Optical absorption spectra of CN nanotube for parallel polarization and perpendicular polarization (gray shaded).

Figure 10. Variation of α_{max} with N concentration in parallel polarization, perpendicular polarization and unpolarized light.

absorption coefficient with N concentration. We depict in figure 10 the variation of the absorption coefficients with N concentration.

It can be seen that the maximum value of the absorption coefficient reaches its highest unique value at a particular concentration of N. Once again, the highest value of the absorption coefficient occurs for parallel polarization of the electromagnetic field. This is in contrast to the case of B doping, where instead of a maximum, a *minimum* value of α_{max} occurs for 40% concentration [48] for the same (8, 0) doped semiconductor SWCNT. Therefore, in this sense, B and N concentration in SWCNTs make quite significant differences in the absorption properties, and this distinguishing feature of B and N concentration in SWCNT may be very helpful in designing optical nano-devices.

3.4. Study of the reflectivity of the C_xN_y system

The reflectivity $R(\omega)$ of any medium at normal incidence is calculated from the refractive indices via the relations (as implemented in CASTEP [51]) given by

$$R(\omega) = \left(\frac{1 - \sqrt{\varepsilon(\omega)}}{1 + \sqrt{\varepsilon(\omega)}} \right)^2, \qquad \varepsilon(\omega) = \varepsilon_1(\omega) + i\varepsilon_2(\omega). \quad (5)$$

It is clearly evident from the definition that the reflectivity is always positive in the scheduled range of the frequency and is dimensionless. R is sometimes regarded as the index of refraction as a function of the wavelength of light used. It is to be remembered that in this calculation we are taking into account the *long wavelength limit* ($q \rightarrow 0$). Thus, we cannot make any prediction about the behavior of reflectivity for any finite value of q. Figure 11 shows the typical reflectivity spectra of a (8, 0) CN tube for perpendicular as well as parallel polarization of the electromagnetic field. In the case of perpendicular polarization of the electromagnetic field, R decreases first reaching a local minimum and then decreases again as ω increases. However, this typical nature of variation
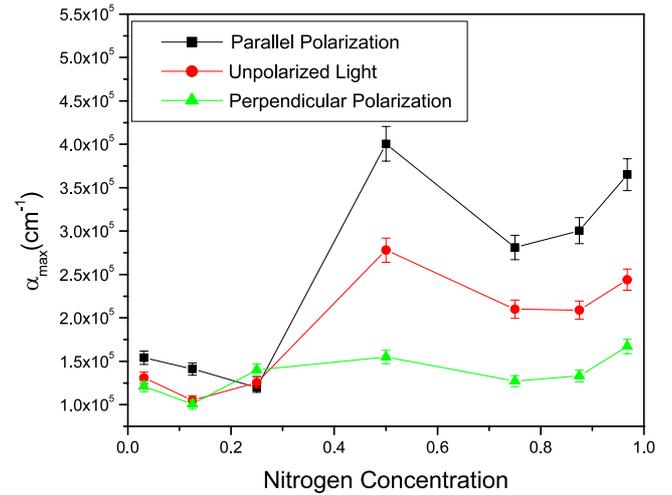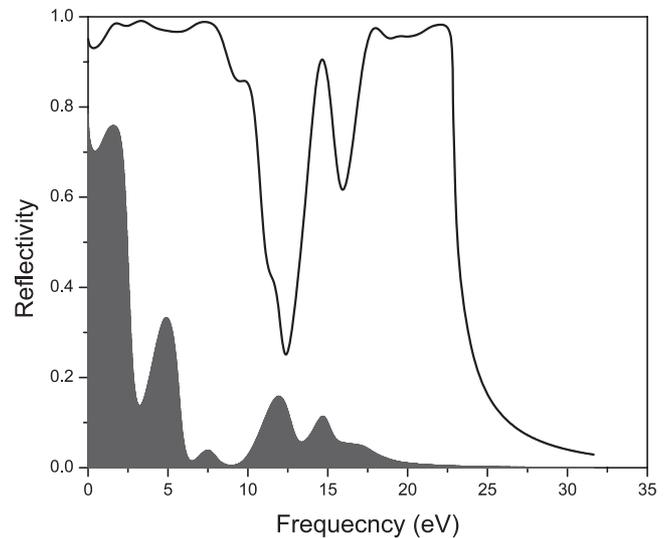

Figure 11. Reflection spectra of a (8, 0) CN tube. The gray shaded is for perpendicular polarization while the other is for parallel polarization.

occurs several times, giving rise to multiple peaks as well as minima. The spectra are, however, for both directions of polarization within 30 eV. For parallel polarization, the values of R are large for the whole range of frequency and some of the peaks are smoothed out. This feature is common to all the N-alloyed SWCNTs. Moreover, near 9 eV we find that the reflectivity vanishes in the case of perpendicular polarization. This can be easily understood from the typical values of the real and imaginary parts of the dielectric constant at the particular frequency. It is to be noted that this fact does not appear for B concentration [50] in the system and hence is to be regarded as a *unique* feature associated with the N-doped (8, 0) system. In figure 12, we show the variation of frequencies at which vanishing of the reflectivities occurs for various N doping concentrations in three cases of electromagnetic field.
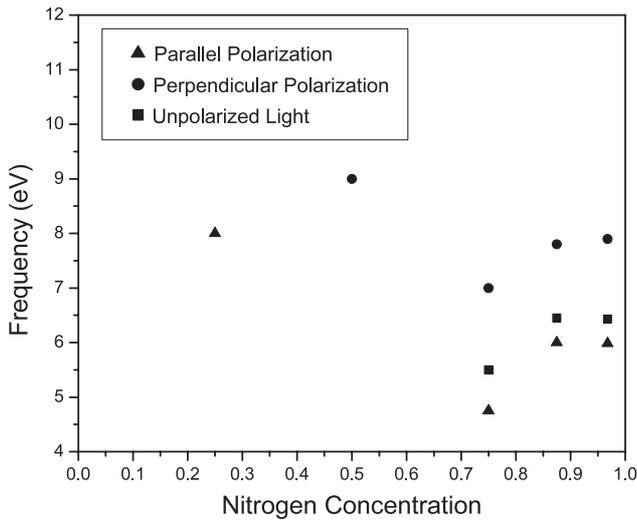
Figure 12. Zero reflectivity at various N concentrations.

It is observed that above 75% concentration, zero reflectivity occurs for all three cases of electromagnetic field.

Only for parallel and perpendicular polarizations does the reflectivity vanish for relatively lower concentrations of N. The respective frequencies all lie in the UV region. This fact may be useful in anti-reflection coatings used for various optical devices. We have also noticed (not shown in the figure) that the static reflectivity, like the dielectric constants, also shows a unique maximum value at a fixed N concentration (50%) for all three cases. However, the maximum values of $R(0)$ are different for each case. We note that the static values of $R(0)$ are not the highest value of the reflectivity, in some cases there exist the other values occurring at a particular finite frequency. The variation of $R_{max}(\omega)$ as a function of N doping in the system (not shown in figure) also shows a similar trend to the static one.
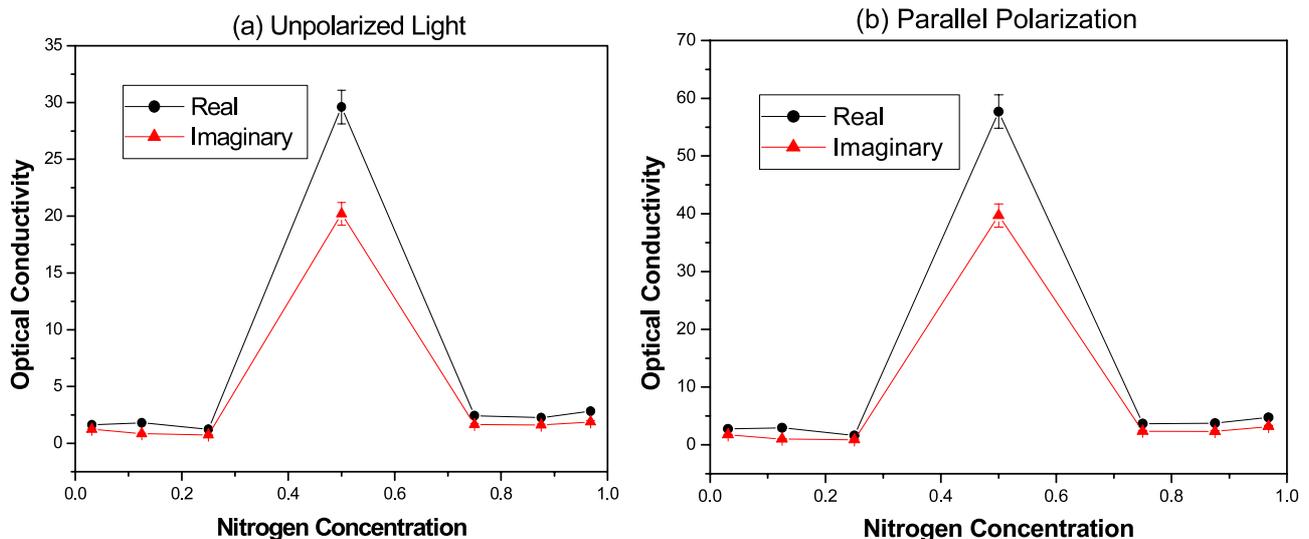
3.5. Study of the optical conductivity of the N-alloyed system

The conductivity $\sigma(\omega)$ is related to the dielectric constant via the relation

$$\sigma(\omega) = \sigma_1 + i\sigma_2 = \frac{-i\omega}{4\pi}(\varepsilon - 1). \qquad (6)$$

The optical conductivity is studied from the dielectric constant with zero DC conductivity and 0.5 eV Drude damping.

In figure 13, we show the variation of the maximum value of the optical conductivity (both real as well as imaginary) with N concentration for parallel polarization and unpolarized light with incidence (1.0, 0.0, 0.0). At 50% concentration, both real and imaginary parts of $\sigma_{max}(\omega)$ show the highest value in the above two electromagnetic field cases. Similar behavior has also been observed in perpendicular polarization. This feature of the optical conductivity results from the typical variation of the dielectric constant (see figure 7). This fact is to be contrasted with that of B concentration in (8, 0) SWCNTs. It was shown [50] that at particular B concentrations, a unique minimum value of $\sigma_{max}(\omega)$ occurs in all three cases. Moreover, in that situation, the values of the concentration at which the minima occur differ in each case, signaling a dependence on the nature of the incident electromagnetic field. A quick look also reveals that the maximum value of the optical conductivity reaches its highest and lowest value in parallel and perpendicular polarization, respectively.

3.6. Study of the loss function of the C_xN_y system

The imaginary part of the reciprocal of the total (real plus imaginary) dielectric constant, being a function of frequency, generally peaks at the plasma frequency. The loss function, which is a direct measure of the collective excitations of the systems, is calculated from $Im[-1/\varepsilon(q, \omega)]$ at $q \rightarrow 0$ limit.

Figure 13. Variation of the optical conductivity with various N concentrations for (a) unpolarized light with incidence direction (1, 0, 0) and (b) parallel polarization.
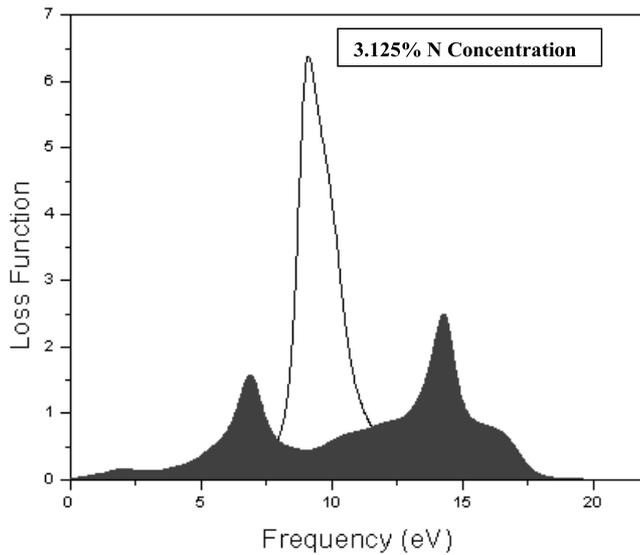
Figure 14. Loss function of a semiconductor (8, 0) $C_{31}N$ SWCNT. The gray shading is for perpendicular polarization while the other is for parallel polarization.

Some straightforward algebra reveals that

$$\text{Im}[-1/\varepsilon(q, \omega)] = \frac{\varepsilon_2(\omega)}{\varepsilon_1^2(\omega) + \varepsilon_2^2(\omega)}. \tag{7}$$

At the plasma frequency, the above expression attains the higher value when $\varepsilon_1 \rightarrow 0$ and $\varepsilon_2 < 1$. HRTEM and nano-EELS can provide information about the systematics and atomic structural defects of N-doped SWCNTs. However, here we are interested in the variation of the peak position as one replaces the C atom(s) by N atom(s).

The loss functions are shown in figure 14 for light polarization parallel and perpendicular to the axis of doped

(8, 0) $C_{31}N$. It can be noticed that there are several peaks apart from a unique significant pronounced one. It was previously observed [46] that in a (8, 0) semiconductor tube the single peak at 9.73 eV was shifted to 9.78 eV on B doping on the CNT for parallel polarization only. It is interesting to note that even replacing one of the C atoms by B or N is enough to change the magnitude of the peak of the loss function as well as its position in the energy spectrum. We notice a pronounced peak at 9.1 eV for parallel polarization. This appearance of a single significant peak (9.5–10 eV) at the long wavelength limit ($q \rightarrow 0$) may be attributed to the typical *unique* collective excitation of π electrons. This value can be compared with the values [59] obtained for π plasmons at the 5.2 eV peak and $\sigma + \pi$ plasmons at 21.5 eV for wavevector of 0.15 Å. However, as seen from figure 14, under perpendicular polarization there are several peaks in the low frequency region (2.1 and 6.90 eV) as well as the high frequency region (14.28 eV). In perpendicular polarization, the appearance of multiple peaks in the loss function implies the existence of various collective excitations involving σ and π electrons in the system. In particular, the high frequency peaks have been attributed to $\pi + \sigma$ plasmons [61]. This can be taken as one of the characteristic features of *any* type of SWCNT in perpendicular polarization. Moreover, the intensities of all the peaks in the case of perpendicular polarization are weaker compared to parallel polarization. This immediately indicates that the π plasmons are not very effective for optical excitations. This fact has been also noticed in the case of MWCNT models [62]. Thus, we conclude that even a small percentage (3.125%) of N concentration can significantly modify the collective excitations of the pure system under various polarization directions. In figure 15, for the sake of comparison, we plot the loss functions of BC and CN nanotubes for parallel polarization of the electromagnetic field.
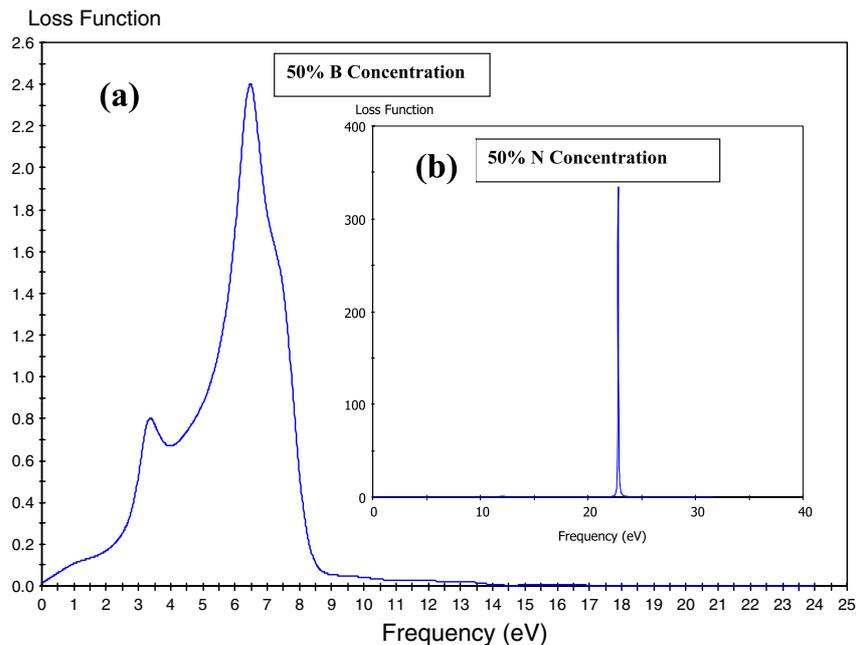

Figure 15. Loss function of a semiconductor (8, 0) (a) BC and (b) CN SWCNT for parallel polarization.
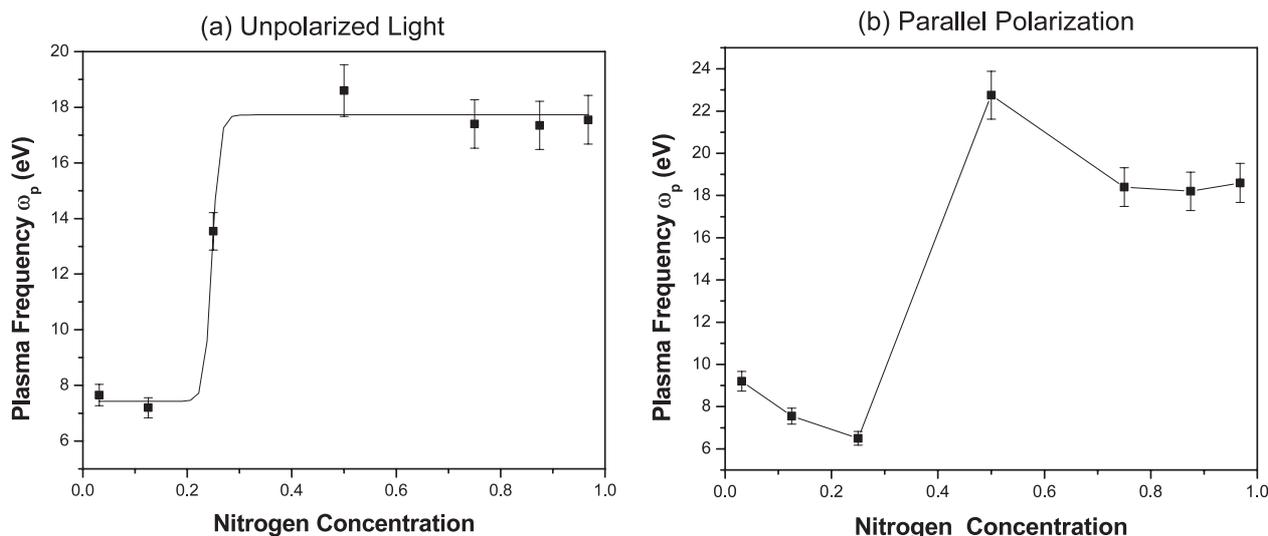
Figure 16. Variation of the plasma resonance frequency with various N concentrations for (a) unpolarized light and (b) parallel polarization.
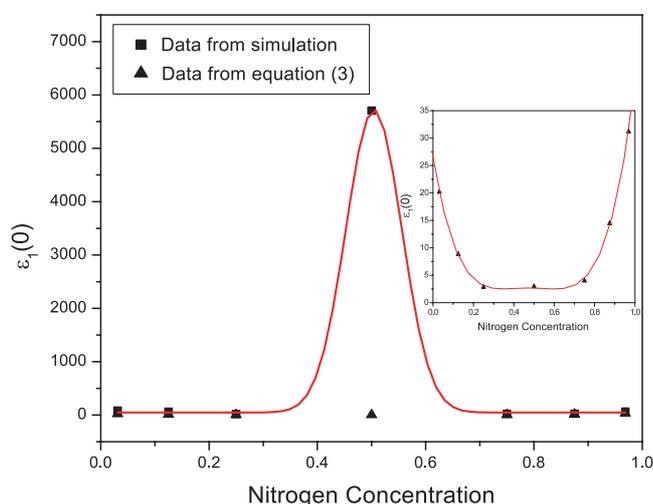

Figure 17. Comparison of the *ab initio* static dielectric constant values with equation (2) for parallel polarization. The inset is the expanded version of the values calculated from equation (2).

A unique sharp peak (with stronger intensity, two orders of magnitude higher) is the characteristic feature of the loss function of a CN nanotube. This is due to the enhanced metallic character of CN nanotubes.

We depict in figure 16 the typical variation of the plasma frequencies of doped (8, 0) SWCNTs computed from the loss function for all three cases with N concentration. The line is a guide to the eye for the variation.

In all three cases, we note that for lower doping concentrations (up to 30% or so) the plasma frequencies do not change appreciably. However, beyond that, the changes in all the cases are quite drastic. For the unpolarized case, between 30 and 50% doping, the plasma frequency shifts to a higher region, and above 50% N concentration the plasma frequencies do not change very significantly. This results in a step like behavior of the plasma frequencies with N concentration. For parallel polarization, however, at 50% doping, the magnitude of the plasma frequency sharply jumps

to a larger one. With further increase in the N concentration, the plasma frequency drops to a lower one, thus indicating a maximum at 50% doping. In the case of B concentration, the plasma resonance frequencies showed a minimum at a particular doping concentration [47] depending on the nature of the electromagnetic field.

With these plasma frequencies and the band gap at the Γ point taken from figure 6, we use equation (2) to calculate the static real dielectric constant. However, it is to be remembered that equation (3) is strictly valid for pure semiconductor SWCNTs. These computed values are compared in figure 17 with simulated *ab initio* values for parallel polarization. These calculated values from equation (2) are less than those of the simulations. In the inset, we show explicitly the variation of the static dielectric constant with N concentration computed from equation (2). The drastic difference of the behavior at 50% doping concentration is to be noted. The simulation shows a maximum at 50% doping, while using equation (2) predicts a minimum. The minimum arises because of the lowest ratio of $\frac{\omega_p}{E_g}$ at 50% N doping concentration. This fact is not observed for a B-doped system [48]. Moreover, all these doped values violate the upper bound restriction as predicted for the pure case [60]. Similar behavior has been observed for both unpolarized as well as perpendicular cases.

The differences in the electronic and optical properties of $B_x C_y$ and $C_x N_y$ are summarized in table 1. Though the results presented above are based on some specific parameter choices, the qualitative gross features of the optical quantity remain unaltered with the change of parameters.

4. Conclusions and perspectives

From the first principles relaxed C–C bond length DFT calculation of the optical property of (8, 0) $C_x N_y$ SWCNT systems, we have observed significant changes in the optical behavior for different N-alloyed CNT systems (radius <1 nm) with different polarizations. The behavior of the static dielectric constant of N-doped systems depends

Table 1. Comparison of electronic and optical properties of B_xC_y and C_xN_y SWCNTs.

Properties	B-alloyed SWCNT	N-alloyed SWCNT
1. Variation of band gap (E_g) at Γ point with doping	Shows a minimum at 55%	Shows a maximum at 57%
2. Static dielectric constant	Minimum at 50% for parallel polarization; minimum at 3.125% for perpendicular polarization; minimum at 12.5% for unpolarized one	Maximum at 50% for all three cases
3. Magnitude of reflectivity	Lower	Higher
4. Zero (vanishing) reflectivity	Does not exist	Does exist at different N concentrations
5. Absorption	Lesser	Higher
6. Maximum absorption coefficient	Minimum at 40% for parallel and perpendicular; 29% for unpolarized	Maximum at 50% for all three cases
7. Magnitude of the loss function	Lesser	Higher
8. Variation of plasma frequency (ω_p) with doping	Shows minimum at 44% for parallel and 33% for unpolarized; no maximum or minimum for perpendicular one	Step function like behavior for unpolarized; maximum at 50% for parallel polarization
9. Ratio of $\frac{\omega_p}{E_g}$	Shows a maximum at 0% (pure) for parallel and 75% doping for unpolarized one	Shows a minimum at 50% doping in all three cases

on the concentration and the nature of polarization of the electromagnetic field. It is observed that the magnitude of the static dielectric constant shows a unique maximum value at 50% doping. The maximum value of the absorption coefficient depends strongly on the concentration of N in a non-linear way as well as on the direction of polarization. The optical conductivity (real as well as imaginary) shows a unique maximum at 50% N doping independent of the direction of polarization. Besides, the vanishing of the reflectivity is seen at some particular concentration of N. In both parallel as well as in unpolarized cases, an enhanced metallic character is noticed from the shifting of the peak of the loss function to a higher frequency. Finally, the variation of the plasma resonance frequency with N concentration indicates the existence of a unique maximum for parallel polarization and a step function like behavior for the unpolarized situation with concentration. It will be interesting to compare the experimental results for a low doping N concentration such as $C_{31}N$ nanotubes.

Acknowledgments

References

[1] Iijima S 1991 Helical microtubules of graphitic carbon *Nature* **354** 56–8
[2] Saito R, Dresselhaus G and Dresselhaus M S 1998 *Physical Properties of Carbon Nanotubes* (London: Imperial College Press)
[3] Reich S, Thomsen C and Maulzsch J 2004 *Carbon Nanotubes: Basic Concepts and Physical Properties* (Weinheim: Wiley–VCH)
[4] Czrew R *et al* 2001 Identification of electron donor states in N-doped carbon nanotubes *Nano Lett.* **1** 457–60
[5] Stephane O *et al* 1994 Doping graphitic and carbon nanotube structures with boron and nitrogen *Science* **266** 1683–5
[6] Borowiak-Palen E, Pichler T, Fuentes G G, Bendjemil B, Liu X, Graff A, Kalenczuk R J, Knupfer M and Fink J 2003 Efficient production of B-substituted single wall carbon nanotubes *Chem. Phys. Lett.* **378** 516
[7] Borowiak-Palen E, Pichler T B, Liu X, Graff A, Kalenczuk R J, Knupfer M and Fink J 2004 Synthesis and electronic properties of B-doped single wall carbon nanotubes *Carbon* **42** 1123–6
[8] Gai Pratibha L, Stephane O, McGuire K, Rao Apparao M, Dresselhaus M S, Dresselhaus G and Colliex C 2004 Structural systematics in boron-doped single wall carbon nanotubes *J. Mater. Chem.* **14** 669–75
[9] Picher T *et al* 2003 Electronic structure and optical properties of boron doped single wall carbon nanotubes *AIP Conf. Proc.* **685** 361–5
[10] Fuentes G G, Borowwiak-Palen E, Knupfer M, Pichler T, Fink J, Wirtz L and Rubio A 2004 Formation and electronic properties of BC_3 single-wall nanotubes upon boron substitution of carbon nanotubes *Phys. Rev.* B **69** 245403–9
[11] Borowiak-Palen E, Picher T, Fuentes G G, Graff A, Kalenczuk R J, Knupfer M and Fink J 2003 Production and characterization of MWBNNT and B-doped SWCNT *AIP Conf. Proc.* **685** 374–7
[12] Graff A, Gemming T, Borowiak-Palen E, Ritschel M, Picher T, Knupfer M and Leonhardt A 2003 Analytical TEM investigation of B doped carbon and BN nanotubes *Microsc. Microanal.* **9** 178–9
[13] Wang R, Zhang D, Zhang Y and Liu C 2006 Boron doped carbon nanotubes serving as a novel chemical sensor for formaldehyde *J. Phys. Chem.* B **110** 18267–71
[14] Sun C-L, Wang H-W, Hayashi M, Chen L-C and Chen K-H 2006 Atomic scale deformation in N-doped carbon nanotubes *J. Am. Chem. Soc.* **128** 8368–9
[15] Chen L-C *et al* 2002 Controlling steps during early stages of the aligned growth of carbon nanotubes using microwave plasma enhanced chemical vapor deposition *Adv. Funct. Mater.* **12** 687–92
[16] Sun C L *et al* 2005 Ultrafine platinum nanoparticles uniformly dispersed on arrayed CN_x nanotubes with high electrochemical activity *Chem. Mater.* **17** 3749–53
[17] Sieh W Z *et al* 1994 Synthesis of $B_xC_yN_z$ nanotubules *Phys. Rev.* B **51** 11229–32
[18] Han W, Cumings J, Huang X, Bradley K and Zettl A 2001 Synthesis of aligned $B_xC_yN_z$ nanotubes by a substitution-reaction route *Chem. Phys. Lett.* **346** 368–72

[19] Liu Y and Guo H 2004 Current distribution in B- and N-doped carbon nanotubes *Phys. Rev.* B **69** 115401–7

[20] Zhou Z, Gao X, Yan J and Song D 2006 Doping effects of B and N on hydrogen adsorption in single wall carbon nanotubes through density functional calculations *Carbon* **44** 939–47

[21] Zhang Z and Cho K 2007 *Ab initio* study of hydrogen interaction with pure and nitrogen doped carbon nanotubes *Phys. Rev.* B **75** 75420–6

[22] Kong J *et al* 2000 Nanotube molecular wires as chemical sensors *Science* **287** 622–5

[23] Peng S and Cho K 2003 *Ab initio* study of doped carbon nanotube sensors *Nano Lett.* **3** 513–7

[24] Bai L and Zhou Z 2007 Computational study of B or N doped single wall carbon nanotubes as NH_3 and NO_2 sensors *Carbon* **45** 2105–10

[25] Yamanioto Y, Kamimura T and Matsumoto K 2005 Nitrogen doping of single walled carbon nanotube by using mass separated low energy ion beams *Japan. J. Appl. Phys.* **44** 1611–4

[26] Loponen T, Krasheninnikov A V, Kaukonen M and Nieminen R M 2006 Nitrogen doped carbon nanotubes under electron irradiation simulated with a tight-binding model *Phys. Rev.* B **74** 73409–13

[27] Carrero-Sainchez J C *et al* 2006 Biocompatibility and toxicological studies of carbon nanotubes doped with nitrogen *Nano Lett.* **6** 1609–16

[28] He M, Zhou S, Zhang J, Liu Z and Robinson C 2005 CVD growth of N-doped carbon nanotubes on Silicon substrate and its mechanism *J. Phys. Chem.* B **109** 9275–9

[29] Lee Y T *et al* 2003 Growth of vertically aligned nitrogen doped carbon nanotubes: control of nitrogen content over the temperature range 900–1100 °C *J. Phys. Chem.* B **107** 12958–63

[30] Chan L H *et al* 2004 Resolution of the binding configuration in nitrogen-doped carbon nanotubes *Phys. Rev.* B **70** 125408–15

[31] Ray S C *et al* 2007 Electronic structures and bonding properties of chlorine-treated nitrogenated carbon nanotubes: x-ray absorption and scanning photo electron microscopy studies *Appl. Phys. Lett.* **90** 12107–9

[32] Kim S Y, Lee J, Na C W, Park J, Seo K and Kim B 2005 N doped double-walled carbon nanotubes synthesized by chemical vapour deposition *Chem. Phys. Lett.* **413** 300–5

[33] Tang C, Bando Y, Goldberg D and Xu F 2004 Structure and nitrogen incorporation of carbon nanotubes synthesized by catalytic pyrolysis of dimethylformamide *Carbon* **42** 2625–33

[34] Cao L M, Zhang X Y, Gao C X, Kang W K, Zhang Z L and Zhang Z 2003 High-concentration nitrogen-doped carbon nanotube arrays *Nanotechnolgy* **14** 931–4

[35] Maldonado S, Morin S and Stevensen K J 2006 Structure, composition and chemical reactivity of carbon nanotubes by selective nitrogen doping *Carbon* **44** 1429–37

[36] Ewels C P and Glerup M 2005 Nitrogen doping in carbon nanotubes *J. Nanosci. Nanotechnol.* **5** 1345–63

[37] Terrones M *et al* 2004 New direction in nanotube science *Mater. Today* **7** 30–45

[38] Yang Q, Xu W, Tomita A and Kyotani T 2005 The template synthesis of double coaxial carbon nanotubes with nitrogen doped and boron doped multiwalls *J. Am. Chem. Soc.* **127** 8956–57

[39] Sharma R B, Late D J, Joag D S, Govindaraj A and Rao C N R 2006 Field emission properties of boron and nitrogen doped carbon nanotubes *Chem. Phys. Lett.* **428** 102–8

[40] Point S, Minea T, Bouchet-Fabre B, Granier A and Turban G 2005 XPS and NEXAFS characterization of plasma deposited vertically aligned N-doped MWCNT *Diamond Relat. Mater.* **14** 891–5

[41] Misra A, Tyagi Pawan K, Singh M K and Misra D S 2006 FTIR studies of nitrogen doped carbon nanotubes *Diamond Relat. Mater.* **15** 385–8

[42] Miyamoto Y, Cohen M L and Louie S G 1997 Theoretical investigation of graphitic carbon nitride and possible tubule forms *Solid State Commun.* **102** 605–8

[43] Villalpando-Paez F, Romero A H, Monoz-Sandoval E, Martinez L M, Terrones H and Terrones M 2004 Fabrication of vapor and gas sensors using films of aligned CN_x nanotubes *Chem. Phys. Lett.* **386** 137–43

[44] Machon M, Reich S, Thomsen C, Sanchez-Portal D and Ordejon P 2002 *Ab initio* calculations of the optical properties of 4 Å-diamater single-walled nanotubes *Phys. Rev.* B **66** 155410–5

[45] Yang X P, Weng H M and Dong J 2003 Optical properties of 4 Å single-walled carbon nanotubes inside zeolite channels studied from first principles calculations *Eur. Phys. J.* B **32** 345–50

[46] Liu H J and Chan C T 2002 Properties of 4 Å carbon nanotubes from first-principles calculations *Phys. Rev.* B **66** 115416–20

[47] Guo G Y, Chen K C, Wang D-S and Duan C-G 2004 Linear and nonlinear optical properties of carbon nanotubes from first-principles calculations *Phys. Rev.* B **69** 205416–26

[48] Jana D, Chen L-C, Chen C W, Chattopadhyay S and Chen K-H 2007 A first principles study of the optical properties of B_xC_y single wall nanotubes *Carbon* **45** 1482–91

[49] Jana D, Chen L-C, Chen C W and Chen K-H 2007 *Ab initio* study of optical conductivity of B_xC_y nano-composite system *Indian J. Phys.* **81** 41–5

[50] Jana D, Chen L-C, Chen C W and Chen K-H 2008 On refractive index and reflectivity of B_xC_y single wall nanotubes: a first principles approach *Asian J. Phys.* at press

[51] Segall M D *et al* 2002 First-principles simulations: ideas, illustration and the CASTEP code *J. Phys.: Condens. Matter* **14** 2717–44

[52] Perdew J P, Berke K and Ernzerhof M 1996 Generalized gradient approximation made simple *Phys. Rev. Lett.* **77** 3865–8

[53] Monkhorst H J and Pack J D 1992 Special points for Brillouin-zone integrations *Phys. Rev.* B **13** 5188–92

[54] Yu S S, Wen Q B, Zheng W T and Jiang Q 2007 Effects of doping nitrogen atoms on the structure and electronic properties of zig-zag single walled carbon nanotubes through first-principles calculations *Nanotechnology* **18** 165702–9

[55] Zhao M, Xia Y, Lewis J P and Zhang R 2003 First-principles calculations for nitrogen-containing single walled carbon nanotubes *J. Appl. Phys.* **94** 2389–402

[56] Zhang G, Duan W H and Gu B L 2002 Effect of substitutional atoms in the tip on field emission properties of capped carbon nanotubes *Appl. Phys. Lett.* **80** 2589–91

[57] Landau L D and Lifshitz E M 1984 *Electrodynamics of Continuous Media* (New York: Pergamon) pp 58–9

[58] Benedict L X, Louie S G and Cohen M L 1995 Static polarizablities of single-wall carbon nanotubes *Phys. Rev.* B **52** 8541–9

[59] Picher T, Knupfer M, Golden M S, Fink J, Rinzler A and Smalley R E 1998 Localized and delocalized electronic states in single-wall carbon nanotubes *Phys. Rev. Lett.* **80** 4729–32

[60] Krupke R, Henrich F, von Löhneysen H and Kappes M M 2003 Separation of metallic from semiconducting single-walled carbon nanotubes *Science* **301** 344–7

[61] Marinopoulos A G, Reining L, Rubio A and Vast N 2003 Optical and loss spectra of carbon nanotubes: depolarization effects and intertube interactions *Phys. Rev. Lett.* **91** 046402–6

[62] Pan H, Feng Y and Lin J 2005 *Ab initio* study of electronic and optical properties of multiwall carbon nanotube structures made up of a single rolled-up graphite sheet *Phys. Rev.* B **72** 085415–20